Kinetic Mechanism of Phenylacetone Monooxygenase from *Thermobifida fusca*[†]

Daniel E. Torres Pazmiño, Bert-Jan Baas, Dick B. Janssen, and Marco W. Fraaije*

Laboratory of Biochemistry, Groningen Biomolecular Sciences and Biotechnology Institute, University of Groningen, Nijenborgh 4, 9747 AG Groningen, The Netherlands

Received November 20, 2007; Revised Manuscript Received January 17, 2008

ABSTRACT: Phenylacetone monooxygenase (PAMO) from *Thermobifida fusca* is a FAD-containing Baeyer-Villiger monooxygenase (BVMO). To elucidate the mechanism of conversion of phenylacetone by PAMO, we have performed a detailed steady-state and pre-steady-state kinetic analysis. In the catalytic cycle (k_{cat} = 3.1 s^{-1}), rapid binding of NADPH (K_d = 0.7 μM) is followed by a transfer of the 4(*R*)-hydride from NADPH to the FAD cofactor (k_{red} = 12 s^{-1}). The reduced PAMO is rapidly oxygenated by molecular oxygen (k_{ox} = 870 mM^{-1} s^{-1}), yielding a C4a-peroxyflavin. The peroxyflavin enzyme intermediate reacts with phenylacetone to form benzylacetate (k_1 = 73 s^{-1}). This latter kinetic event leads to an enzyme intermediate which we could not unequivocally assign and may represent a Criegee intermediate or a C4a-hydroxyflavin form. The relatively slow decay (4.1 s^{-1}) of this intermediate yields fully reoxidized PAMO and limits the turnover rate. $NADP^+$ release is relatively fast and represents the final step of the catalytic cycle. This study shows that kinetic behavior of PAMO is significantly different when compared with that of sequence-related monooxygenases, e.g., cyclohexanone monooxygenase and liver microsomal flavin-containing monooxygenase. Inspection of the crystal structure of PAMO has revealed that residue R337, which is conserved in other BVMOs, is positioned close to the flavin cofactor. The analyzed R337A and R337K mutant enzymes were still able to form and stabilize the C4a-peroxyflavin intermediate. The mutants were unable to convert either phenylacetone or benzyl methyl sulfide. This demonstrates that R337 is crucially involved in assisting PAMO-mediated Baeyer-Villiger and sulfoxidation reactions.

During the past few decades, a number of microbial monooxygenases have been described that are able to perform the insertion of an oxygen atom in (a)cyclic ketones, yielding the corresponding esters or lactones. Most of these Baeyer-Villiger monooxygenases (BVMOs)[1] are sequence-related and have been classified as type I BVMOs. Biochemical studies have shown that these monooxygenases are also able to oxidize sulfur, nitrogen, and boron atoms (*1*). For the oxidation of organic substrates, type I BVMOs employ FAD as a prosthetic group, NADPH as an electron donor, and molecular oxygen as an oxidant. So far, the most extensively studied BVMO is cyclohexanone monooxygenase (CHMO, EC 1.14.13.16) from *Acinetobacter* sp. NCIMB 9871 (*2–7*). An initial kinetic study of this enzyme was performed in the early 1980s, followed by a more detailed study in 2001 by Sheng and co-workers (*8, 9*). On the basis of these and other studies on BVMOs, it has become clear that the ability to catalyze a Baeyer-Villiger oxidation relies on the formation and stabilization of a C4a-peroxyflavin during the catalytic cycle. This strong oxidant is formed by NADPH-mediated reduction and subsequent oxygenation of the FAD cofactor. The C4a-peroxyflavin is proposed to perform a nucleophilic attack on the carbonyl group of the substrate. This yields a Criegee adduct in which the substrate is covalently bound to the flavin cofactor. Spontaneous rearrangement of this flavin intermediate eventually results in the formation of the Baeyer-Villiger product and a C4a-hydroxyflavin intermediate. Dehydration of the latter flavin intermediate produces the oxidized flavin and completes the catalytic cycle.

For CHMO, it has been shown that the C4a-peroxyflavin intermediate can be formed and stabilized in the absence of an organic substrate. Only in a relatively slow process does this reactive enzyme intermediate decay to form hydrogen peroxide (*8*). Thus, in the absence of a suitable substrate, BVMOs act as inefficient NADPH oxidases. Until recently, the mechanism by which BVMOs elicit formation of the C4a-peroxyflavin and are able to stabilize this labile intermediate has remained enigmatic as no structural information for CHMO or a related monooxygenase was available. By 2005, however, phenylacetone monooxygenase (PAMO, EC 1.14.13.92) from *Thermobifida fusca* had been discovered (*10*). The enzyme is sequence-related to several known BVMOs, e.g., cyclohexanone monooxygenase (*4*) and ethionamide monooxygenase (*11*). PAMO contains a tightly bound FAD as a cofactor and uses NADPH as an electron donor. The best substrate identified so far is phenylacetone which undergoes a Baeyer-Villiger oxidation yielding benzylacetate. Also, other ketones and aldehydes are accepted by the monooxygenase. Moreover, it is able to catalyze (enantioselective) sulfoxidations and N-oxidations (*12*). Features that make this BVMO particularly interesting for biotechnological applications are its thermostability and tolerance toward high

[†] We thank CERC3 for funding. COST D25/0005/03 is gratefully acknowledged.

* To whom correspondence should be addressed. Phone: (31) 50-3634345. Fax: (31) 50-3634165. E-mail: M.W.Fraaije@rug.nl.

[1] Abbreviations: PAMO, phenylacetone monooxygenase; CHMO, cyclohexanone monooxygenase; BVMO, Baeyer-Villiger monooxygenase; FMO, flavin-containing monooxygenase.

10.1021/bi702296k CCC: $40.75
Published on Web 03/06/2008

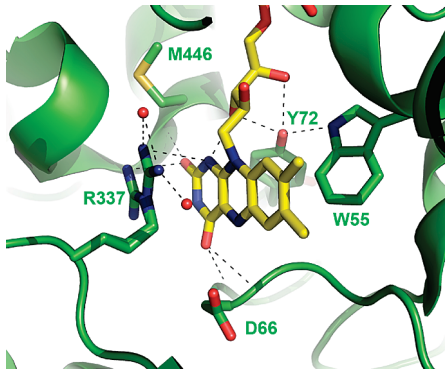

FIGURE 1: Representation of the active site of phenylacetone monooxygenase. The FAD cofactor is shown in yellow sticks, while several active side residues and water molecules are highlighted (in green sticks and red spheres, respectively). For R337, both side chain orientations that are observed in the crystal structure are shown (PDB entry 1W4X). Hydrogen bonds around the flavin are represented by dashed lines. The figure was prepared using PyMol (www.pymol.org).

concentrations of organic solvents (*13*). Remarkably, the use of specific solvents can even increase the enantioselectivity of the enzyme (*14*). The elucidation of the crystal structure of PAMO, as yet representing the only available BVMO structure, has revealed structural details of this monooxygenase (*15*). The active site is located between two domains, an FAD binding domain and a NADPH binding domain. On the basis of the structure, it has been proposed that during catalysis the active site residue R337 adopts several conformations while domain rearrangements are also predicted to play a role. The PAMO structure has triggered several structure-inspired enzyme redesign studies on PAMO and sequence-related BVMOs (*16–19*).

Now that the crystal structure of PAMO is available, it is possible to identify residues that may assist in catalysis. One of these residues is R337, which is located near the bound FAD cofactor with its guanidinium side chain only 3.7 Å from the *re* face of the planar aromatic system of the cofactor (*15*) (Figure 1). Amino acid sequence alignment of (putative) type I BVMOs shows that this arginine is strictly conserved (*20, 21*). Replacement of the corresponding arginine in 4-hydroxyacetophenone monooxygenase (HAPMO) from *Pseudomonas fluorescens* ACB resulted in the inactivation of the enzyme (*22*). It has been suggested that R337 in PAMO is involved in the stabilization of the negatively charged C4a-peroxyflavin (*15*). In this paper, we report the investigation of the kinetic properties of PAMO with the goal of improving our understanding of BVMO-mediated catalysis. A detailed steady-state and pre-steady-state kinetic analysis of wild-type PAMO and two mutants, R337A and R337K, is presented.

MATERIALS AND METHODS

Materials. (*R*)-NADPD was prepared using a $NADP^+$-dependent alcohol dehydrogenase from *Thermoanaerobacter brockii* (*23*). On the basis of an A_{260}/A_{340} ratio of 2.8, the purity of the deuterated coenzyme was estimated to be >80%. All chemicals and enzymes were obtained from ACROS Organics, Jülich Fine Chemicals, Roche Applied Sciences, or Sigma-Aldrich. Oligonucleotide primers were obtained from Sigma Genosys. DNA sequencing was conducted at GATC (Konstanz, Germany).

Site-Directed Mutagenesis. For mutagenesis, the previously constructed plasmid pPAMO was used (*10*). The plasmid contains the *pamo* gene (GenBank accession number YP_289549) under control of the P_{BAD} promoter. Mutants were constructed using the QuickChange site-directed mutagenesis kit from Stratagene with pPAMO as the template following the recommendations of the manufacturer. R337 was mutated to an alanine or lysine with primer 5′-TTCGGCACCAAG**GCC**CTCATCCTGGAA-3′ or 5′-TTCGGCACCAAG**AAA**CTCATCCTGGAA-3′ and their complementary primers, respectively. The mutated codons are shown in bold.

Growth of Bacterial Cells and Enzyme Purification. Wild-type His-tagged PAMO was expressed in *Escherichia coli* TOP10 cells and purified as described previously (*10*). Both PAMO mutants were also expressed in *E. coli* TOP10 cells using the same conditions that were used for wild-type PAMO but purified by means of the following procedure. *E. coli* TOP10 cells from a 500 mL culture were harvested by centrifugation and resuspended in 20 mL of 50 mM Tris-HCl (pH 7.5). After sonication, FAD was added to a final concentration of 50 μM and the ruptured cells were incubated at 50 °C for 1 h and subsequently centrifuged. All further steps were carried out at 4 °C. The resulting supernatant was applied to a Q-Sepharose column (50 mL; Amersham Biosciences). The protein was eluted using a linear gradient increasing from 0 to 1 M KCl [in 50 mM Tris-HCl (pH 7.5)]. The mutant enzymes were further purified by means of size-exclusion chromatography using a Superdex 200 column (330 mL; Amersham Biosciences). The concentration of wild-type PAMO was determined by measuring the absorbance at 441 nm using an extinction coefficient of 12.4 mM^{-1} cm^{-1} (*10*). The extinction coefficients of both mutants were determined by comparing the flavin spectrum of the purified enzymes with the flavin spectrum obtained after unfolding with 0.1% SDS. This resulted in the extinction coefficients for PAMO R337A (ϵ_{441} = 12.8 mM^{-1} cm^{-1}) and PAMO R337K (ϵ_{440} = 12.1 mM^{-1} cm^{-1}).

Steady-State Kinetics. The activities of the purified enzymes were determined spectrophotometrically by monitoring the decrease in the level of NADPH over time at 340 nm (ϵ_{340} = 6.22 mM^{-1} cm^{-1}). The reaction mixture (1.0 mL) typically contained 50 mM Tris-HCl (pH 7.5), 100 μM NADPH, 1.0 mM phenylacetone, 1% (v/v) DMSO, and 0.05–1 μM enzyme. The inhibition constant of $NADP^+$ toward wild-type PAMO was determined by performing steady-state kinetic experiments in the presence of 0–8 μM $NADP^+$. These kinetic measurements were performed on a Perkin-Elmer Lambda Bio40 spectrophotometer. The steady-state kinetic parameters with oxygen were determined by measuring the oxygen depletion in a 1 mL stainless steel stirred vessel equipped with an optical MOPS-1 oxygen sensor (Compte, Hannover, Germany) and fitting the obtained depletion curve with eq 1 by means of numerical integration (Micromath Scientist, version 2.0).

$$\frac{d[O_2]}{dt} = \frac{k_{cat}[E]_0[O_2]}{K_M + [O_2]} \quad (1)$$

The relative flavin absorbance of wild-type PAMO and the mutants during steady-state catalysis was determined by monitoring the absorbance at 441 nm over time using an Applied Photophysics SX17MV stopped-flow apparatus. For

this, 8 μM enzyme was aerobically mixed with 800 μM NADPH, 2 mM phenylacetone, and 2% (v/v) DMSO in either 50 mM PIPES buffer (pH 6–7) or 50 mM Tris-HCl buffer (pH 7–9). As a reference, the absorbance of fully oxidized PAMO was set at 100%, while the absorbance of anaerobically reduced PAMO was set at 0%.

Pre-Steady-State Kinetics. Both the reductive and oxidative half-reactions of PAMO and the mutants were analyzed using the stopped-flow apparatus. All experiments described below were performed at 25 °C in 50 mM Tris-HCl (pH 7.5). Anaerobic conditions were achieved by flushing the system and solutions with N_2 and removing traces of oxygen upon addition of 10 mM glucose and a catalytic amount of glucose oxidase.

Reduction of PAMO by NADPH or (*R*)-NADPD was assessed anaerobically at various concentrations of the nicotinamide coenzyme using a photodiode array detector. The obtained spectra were analyzed by means of numerical integration methods using Pro-K (Applied Photophysics Ltd.), yielding the observed rate constants. The binding and oxidation of NADPH or (*R*)-NADPD were assessed by following the fluorescence (λ_{ex} = 340 nm, band pass filter WG 375 nm) over time under anaerobic conditions. The obtained data could be fitted using eq 2.

Single-wavelength studies at 380 nm were used to determine the rate of oxygenation of the reduced enzymes. For this, PAMO was anaerobically reduced using equimolar amounts of NADPH outside the stopped-flow apparatus in the presence of 36 μM $NADP^+$. The reoxidation of the C4a-peroxyflavin intermediate in the absence and presence of phenylacetone was measured using a photodiode array detector. Reduced PAMO, prepared as described for the single-wavelength studies, was mixed with aerated buffer containing various concentrations of phenylacetone (0–4 mM). As for the solution containing reduced PAMO, 36 μM $NADP^+$ was added to maintain a constant $NADP^+$ concentration after mixing, thereby preventing possible release of $NADP^+$. The reoxidation of the C4a-peroxyflavin intermediate at various pH values was carried out by mixing it with either 50 mM PIPES (pH 6–7) or 50 mM Tris-HCl (pH 7–9) buffer containing 2 mM phenylacetone, 36 μM $NADP^+$, and 2% (v/v) DMSO. Analysis of the obtained spectra was performed as described above for the reduction of PAMO by the coenzyme.

The affinity for $NADP^+$ ($K_{d,NADP^+}$) was determined by measuring the change in the flavin absorbance spectrum upon titration of 66 μM PAMO with 0–514 μM $NADP^+$.

Product Identification. To determine whether the PAMO mutants were able to convert phenylacetone or benzyl methyl sulfide, the reaction was analyzed by means of gas chromatography. For product identification, reaction mixtures contained 2.5 mM substrate, 100 μM NADPH, 5 mM glucose 6-phosphate, 2.5 units of glucose-6-phosphate dehydrogenase, and 0.5 μM enzyme (*13, 24*).

Data Analysis. Stopped-flow fluorescence traces of the nicotinamide coenzyme binding and enzyme reduction were fitted using nonlinear regression analysis to a double-exponential equation, resulting in two different observed rates (k_{obs1} and k_{obs2}) for different coenzyme concentrations.

$$F = ae^{-k_{obs1}t} + be^{-k_{obs2}t} + c \quad (2)$$

Scheme 1: Reduction of PAMO by NADPH

$$E_{ox} \underset{k_{off}}{\overset{k_{on}[NADPH]}{\rightleftharpoons}} E_{ox}\sim NADPH \underset{k_{rox}}{\overset{k_{red}}{\rightleftharpoons}} E_{red}\sim NADP^+$$

The individual rate constants in Scheme 1 were obtained by fitting eqs 3 and 4 (*25*) to the experimental k_{obs} values using nonlinear regression analysis (SigmaPlot version 10.0 for Windows).

$$k_{obs} = k_{off} + k_{on}[NADPH] \quad (3)$$

$$k_{obs2} = k_{rox} + \frac{k_{red}[NADPH]}{[NADPH] + K_{d,app}} \text{ in which}$$

$$K_{d,app} = K_{d,NADPH} + \frac{k_{red}}{k_{on}} \quad (4)$$

Fitting the absorbance traces of the oxygenation reaction to a single-exponential equation resulted in k_{obs} values for different oxygen concentrations. By fitting eq 5 to the experimental k_{obs} values, we obtained the individual rate constant for oxygenation of the reduced enzyme (k_{ox}).

$$F = ae^{-k_{obs1}t} + c \quad (5)$$

The experimental observed rates for the first reoxidation step using phenylacetone as the substrate increased hyperbolically with increasing substrate concentration and could be fitted with eq 6 using nonlinear regression analysis (SigmaPlot version 10.0 for Windows).

$$k_{obs} = \frac{k_{BV}[PA]}{[PA] + K_{PA}} \quad (6)$$

Derivation of Steady-State Parameters from Kinetic Constants. Mathematica version 5.2 was used to derive rate equations from the kinetic scheme by the determinant method (see the Supporting Information for details). The kinetic parameters k_{cat}, $K_{M,NADPH}$, $K_{M,oxygen}$, and $K_{M,PA}$ can be calculated according to the following equations.

$$k_{cat} = \frac{k_{red}k_{BV}k_ck_{ox}[O_2]}{(k_{BV}k_c + k_{red}k_c + k_{red}k_{BV})k_{ox}[O_2] + k_{red}k_{BV}k_c} \quad (7a)$$

$$K_{M,NADPH} = \frac{k_{BV}k_cK_{d,NADPH}k_{ox}[O_2]}{(k_{BV}k_c + k_{red}k_c + k_{red}k_{BV})k_{ox}[O_2] + k_{red}k_{BV}k_c} \quad (7b)$$

$$K_{M,O_2} = \frac{k_{red}k_{BV}k_c}{k_{BV}k_ck_{ox} + k_{red}k_ck_{ox} + k_{red}k_{BV}k_{ox}} \quad (7c)$$

$$K_{M,PA} = \frac{k_{red}k_cK_{d,PA}k_{ox}[O_2]}{(k_{BV}k_c + k_{red}k_c + k_{red}k_{BV})k_{ox}[O_2] + k_{red}k_{BV}k_c} \quad (7d)$$

These equations could be simplified by calculating the catalytic efficiency of the enzyme for substrates NADPH and phenylacetone:

$$\frac{k_{cat}}{K_{M,NADPH}} = \frac{k_{red}k_{on}}{k_{off}} \quad (7e)$$

$$\frac{k_{cat}}{K_{M,PA}} = \frac{k_{BV}}{K_{d,PA}} \quad (7f)$$

Additionally, the relative absorbance at 441 nm during steady state could be derived mathematically from the

concentrations of the various enzyme species obtained by the determinant method.

$$A_{441} = \frac{A_1[E_{ox,total}] + A_2[E_{red}{-}NADP^+] + A_3[E_{per,total}] + A_4[E_{ox}{-}NADP^+]}{(A_1 + A_2 + A_3 + A_4)[E_{total}]} \quad (7g)$$

in which A_1, A_2, A_3, and A_4 represent the relative absorption of each enzyme species.

Table 1: Steady-State Kinetic Parameters of Wild-Type PAMO

	measured	calculated[a]
NADPH as the Coenzyme		
k_{cat} (s^{-1})	3.1 ± 0.2	3.0
$K_{M,coenzyme}$ (μM)	0.7 ± 0.1	0.1
$K_{M,PA}$ (μM)	80 ± 6	30
$K_{M,oxygen}$ (μM)	10 ± 4	3.4
$K_{I,NADP^+}$ (μM)	2.7 ± 1.0	nd[b]
$K_{I,BA}$ (μM)	>5000	nd[b]
A_{441} (%)	68	71
(*R*)-NADPD as the Coenzyme		
k_{cat} (s^{-1})	0.9 ± 0.2	1.5
$K_{M,coenzyme}$ (μM)	0.4 ± 0.1	0.4
A_{441} (%)	80	85

[a] Kinetic parameters were calculated using the determinant method (see the Supporting Information). [b] Not determined.

RESULTS

Steady-State Kinetics. The steady-state kinetic parameters of wild-type PAMO were determined in aerated 50 mM Tris-HCl (pH 7.5) at 25 °C. Using phenylacetone and NADPH as substrates, PAMO exhibited typical Michaelis−Menten behavior, yielding the catalytic (k_{cat}) and Michaelis constants (K_M) for both substrates. By measuring the depletion of molecular oxygen in a closed reaction vessel, we could also obtain the kinetic parameters of the enzyme toward this third substrate (Table 1). In a stopped-flow apparatus, the relative absorbance of the flavin cofactor (A_{441}) during catalysis was monitored. In the presence of saturating concentrations of NADPH, oxygen, and phenylacetone, this absorbance was found to be 68% of the fully oxidized flavin absorbance during steady-state catalysis. This indicates that most of the enzyme is present in an oxidized state.

The inhibitory effects of the products benzylacetate and $NADP^+$ were also determined. Benzylacetate was found to show no inhibition when used at concentrations of up to 5.0 mM. On the other hand, the oxidized nicotinamide coenzyme ($NADP^+$) caused strong competitive inhibition ($K_{I,NADP^+}$ = 2.7 ± 1.0 μM). Similar results were previously found for CHMO, in which $NADP^+$ also acted as a competitive inhibitor and the oxygenated product ϵ-caprolactone did not affect the activity of the enzyme (*8*). $NADP^+$ is also a competitive inhibitor of hydroxyacetophenone monooxygenase (HAPMO) from *P. fluorescens* ACB. For this enzyme, recent mass spectrometry measurements provided direct proof that $NADP^+$ remains bound during catalysis (*26*). Also, the crystal structure of PAMO has revealed that the enzyme contains a binding pocket which can accommodate NADPH or $NADP^+$.

In the absence of phenylacetone, PAMO consumed NADPH at a rate (0.02 s^{-1}) that was 150-fold lower than the k_{cat}. During this nonproductive form of catalysis, also termed the uncoupling reaction, only NADPH and molecular oxygen are consumed, thereby yielding $NADP^+$ and hydrogen peroxide.

To gain additional insight into the mechanism of reduction of flavin by NADPH, we performed additional steady-state kinetic studies using deuterated coenzyme (*R*)-NADPD. Compared to that with the nondeuterated coenzyme, the Michaelis constant was found to be hardly affected (Table 1). On the other hand, k_{cat} measurements showed that deuteration of the coenzyme resulted in a significant kinetic isotope effect (KIE = 3.4). This indicates that the (*R*)-hydrogen of NADPH is transferred as a hydride to the flavin cofactor. Furthermore, it was found that the enzyme was predominantly (80%) present in the oxidized state, compared to 68% when using NADPH as the coenzyme. This further indicates that the overall rate of catalysis is largely determined by the rate of hydride transfer upon replacement of NADPH by (*R*)-NADPD as the coenzyme.

Reductive Half-Reaction. Flavoprotein oxidoreductases are enzymes that catalyze redox reactions, and their mechanism of action can be subdivided into two half-reactions, a reductive half-reaction and an oxidative half-reaction. In the case of type I BVMOs, the reduction of the FAD cofactor by NADPH is considered the reductive half-reaction. To determine individual rate constants for this half-reaction, the stopped-flow technique was used with PAMO. The anaerobic reduction of 8 μM wild-type PAMO by 50 μM NADPH was monitored over time using the stopped-flow apparatus equipped with a photodiode array detector. The collected spectral scans could be fitted best with a two-step model (A $\rightleftarrows$ B $\rightarrow$ C). The typical oxidized flavin absorbance spectrum disappeared over time during the first phase, which represents the reversible reduction of the enzyme. This occurred with rate constants of 11.8 ± 0.1 s^{-1} (flavin reduction) and 1.4 ± 0.3 s^{-1} (flavin reoxidation). The second process (1.6 ± 0.3 s^{-1}) exhibited less pronounced spectral changes (Figure 2), and the difference spectrum of species B and C suggests formation of a small amount of a peroxyflavin species. We propose that this reflects the slow reaction of reduced flavin with small quantities of molecular oxygen that is still present in the system (from the k_{ox} mentioned below, it was estimated that ~1 μM O_2 was still present in the system). The observed rates for the reduction and reoxidation of the flavin (A $\rightleftarrows$ B) were found to be independent of the concentration of the coenzyme in the range of 25−100 μM NADPH. Additionally, no changes in the amplitude and spectral properties of the deconvoluted enzyme intermediates were observed. This suggests that the $K_{d,NADPH}$ is well below 25 μM and that flavin reduction (k_{red}) and reoxidation (k_{rox}) occur at rates of 11.8 ± 0.1 and 1.4 ± 0.3 s^{-1}, respectively. No step prior to enzyme reduction was observed, indicating that the binding of NADPH is fast (>500 s^{-1} in the presence of 25 μM NADPH) and/or has hardly any effect on the flavin absorption spectrum. Furthermore, by performing these experiments in the presence of phenylacetone (up to 1 mM), we observed that the rate of reduction was not affected by the organic substrate.

To study the binding of NADPH to the enzyme, which was not resolved from flavin reduction using the stopped-flow absorbance measurements described above, we exploited the fluorescence properties of NADPH. This made

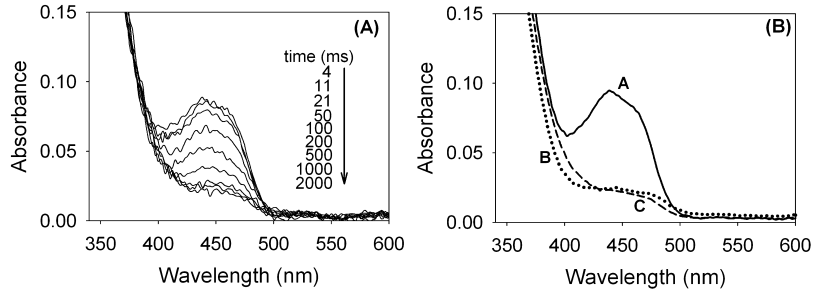

FIGURE 2: (A) Some selected flavin absorbance spectra observed during anaerobic reduction of 8 μM wild-type PAMO by 50 μM NADPH (50 mM Tris-HCl at pH 7.5 and 25 °C). Of all 1600 recorded spectra, only spectra recorded at the indicated times are shown. (B) Spectra of the deconvoluted enzyme species. By means of numerical integration (Pro-K, Applied Photophysics Ltd.), the spectra were fitted using a two-step kinetic model (A $\rightleftarrows$ B $\rightarrow$ C).

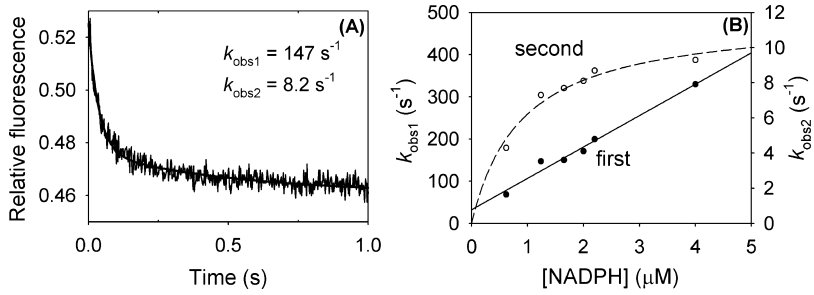

FIGURE 3: Kinetic analysis of the fluorescence traces obtained after anaerobic mixing of wild-type PAMO and NADPH (50 mM Tris-HCl at pH 7.5 and 25 °C). (A) Observed fluorescence trace upon mixing 0.12 μM PAMO with 1.25 μM NADPH. The solid line shows the fit using a double-exponential equation, yielding k_{obs1} and k_{obs2}. (B) The black circles (●) and the solid line (—) show the observed rates (k_{obs1}) of the first step at various NADPH concentrations and the corresponding linear fit, respectively (k_{off} = 32 ± 12 s^{-1}; k_{on} = 74 ± 5 μM^{-1} s^{-1}). The white circles (○) and the dashed line (---) show the observed rates of the second step (k_{obs2}) at various NADPH concentrations and the corresponding fit, respectively. The maximum rate (k_{red}) was determined to be 11.8 ± 0.9 s^{-1}.

it possible to perform stopped-flow experiments at low enzyme concentrations. Reducing 0.12 μM PAMO with various concentrations of NADPH (0.6–4 μM) under anaerobic conditions resulted in fluorescence traces consisting of two phases which were completed within 2 s of mixing (Figure 3A). The observed rates for the fast phase increased linearly with increasing coenzyme concentrations and varied from 68 to 330 s^{-1} (Figure 3B). The high rates of the fast phase observed in the fluorescence traces, which are up to 28-fold higher than the reduction rate described above, suggest that this fast process represents the binding of NADPH to the enzyme, yielding the E_{ox}−NADPH complex (Scheme 1) in which the fluorescence of the coenzyme is quenched. Linear fitting of these k_{obs} values with eq 3 yielded the individual rate constants for the association (k_{on} = 74 μM^{-1} s^{-1}) and dissociation (k_{off} = 32 s^{-1}) of NADPH (Table 2). The values confirm the high affinity of PAMO for NADPH, as the calculated binding constant ($K_{d,NADPH}$) is 0.4 ± 0.2 μM. The observed rates for the second and slower phase displayed a hyperbolic NADPH concentration dependence with rates ranging from 4 to 10 s^{-1}. This indicates that the second process is most likely the oxidation of NADPH to $NADP^+$ coupled with reduction of the flavin. This is in agreement with a decrease in fluorescence. Fitting the observed rates of the second phase with eq 4 yielded an apparent affinity ($K_{d,app}$) of 0.9 ± 0.2 μM and a maximum rate of 11.8 ± 0.9 s^{-1}. This is in line with the $K_{d,NADPH}$ being below 1 μM, as calculated using the association and dissociation constants (see above).

Kinetic Isotope Effect on the Reductive Half-Reaction. As mentioned above, the use of (*R*)-NADPD as the coenzyme resulted in a significant decrease in the overall catalytic rate. To measure the KIE on the rate of reduction, 8 μM PAMO was anaerobically reduced by 50 μM (*R*)-NADPD using the stopped-flow instrument equipped with a photodiode array detector. This resulted in a relatively slow reduction of the enzyme. As described above for reduction with NADPH, the absorption data could be fitted best using a two-step model in which the first step is reversible (see the Supporting Information for details). This resulted in deconvoluted enzyme intermediates with the same spectral properties as those shown in Figure 2B. Reduction and reoxidation of the FAD cofactor were found to occur at rates of 2.1 ± 0.1 and 0.5 ± 0.1 s^{-1}, respectively. The second process was again relatively slow (<0.1 s^{-1}) and was ascribed to the presence of small amounts of O_2 in the mixing chamber. The 6-fold decrease in the reduction rate using (*R*)-NADPD instead of

Table 2: Individual Kinetic Rate Constants and Dissociation Constants Describing the Catalytic Cycle of Wild-Type PAMO and Mutants R337A and R337K

reductive half-reaction		oxidative half-reaction	
	Wild-Type PAMO		
k_{on} (μM^{-1} s^{-1})	74 ± 5	k_{ox} (mM^{-1} s^{-1})	870 ± 35
k_{off} (s^{-1})	32 ± 12	K_{PA} (μM)	730 ± 50
$K_{d,NADPH}$ (μM)	0.7 ± 0.3	k_1 (s^{-1})	73 ± 1
k_{red} (s^{-1})	11.8 ± 0.1	k_2 (s^{-1})	4.1 ± 0.1
k_{rox} (s^{-1})	1.4 ± 0.3	k_{unc} (s^{-1})	0.014
$K_{d,NADP^+}$ (μM)	3.3 ± 0.3		
	PAMO R337A		
k_{on} (μM^{-1} s^{-1})	145 ± 30	k_{ox} (mM^{-1} s^{-1})	46 ± 2
k_{off} (s^{-1})	57 ± 20	k_{unc} (s^{-1})	0.001
k_{red} (s^{-1})	0.12 ± 0.01		
	PAMO R337K		
k_{on} (μM^{-1} s^{-1})	nd[a]	k_{ox} (mM^{-1} s^{-1})	51 ± 2
k_{off} (s^{-1})	nd[a]	k_{unc} (s^{-1})	0.002
k_{red} (s^{-1})	0.07 ± 0.01		

[a] Not determined.

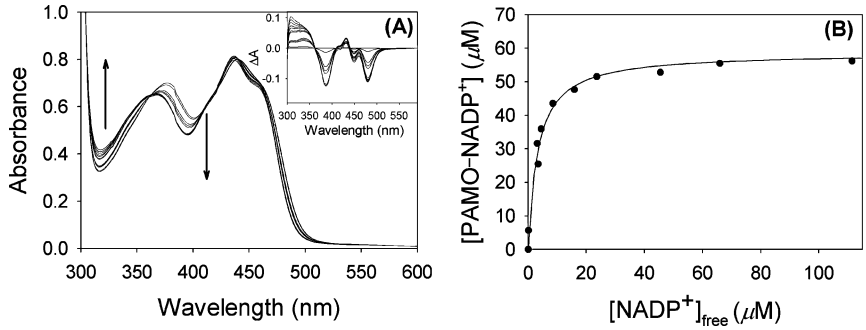

FIGURE 4: (A) Flavin absorbance spectra of 66 μM PAMO upon titration with NADP$^+$ (25 °C in 50 mM Tris-HCl at pH 7.5). The concentration of NADP$^+$ was varied from 0 to 514 μM. The inset shows the difference spectra of PAMO upon titration with NADP$^+$ using the spectrum of PAMO with no NADP$^+$ as a reference. (B) NADP$^+$ binding affinity for wild-type PAMO. The relationship between the concentration of the formed PAMO–NADP$^+$ complex and free NADP$^+$ using different initial concentrations of NADP$^+$ indicates a high binding affinity. Nonlinear regression of the ΔA_{387} data using the data from panel A indicated that wild-type PAMO has an apparent binding affinity for NADP$^+$ of 3.3 $\pm$ 0.3 μM, which is equal to the inhibition constant for NADP$^+$ ($K_{I,NADP^+}$).

NADPH as the coenzyme confirms that PAMO preferably accepts the 4(*R*)-hydrogen of the coenzyme. A low k_{red} is also in agreement with the previously determined increase in A_{441} during steady-state turnover using (*R*)-NADPD, which reflects the fact that a larger fraction of the enzyme is present in the oxidized state during catalysis.

The change in (*R*)-NADPD fluorescence over time showed traces similar to those obtained with NADPH. Anaerobic reduction of 0.12 μM PAMO by 0.9–3.0 μM (*R*)-NADPD revealed again a decrease in fluorescence consisting of two phases (see the Supporting Information for details). As for the reductive half-reaction with NADPH, the observed rates for the fast phase increased linearly with an increase in coenzyme concentration, resulting in similar rate constants for association (k_{on} = 47 μM^{-1} s^{-1}) and dissociation (k_{off} = 35 s^{-1}) of (*R*)-NADPD, yielding a $K_{d,NADPD}$ of 0.7 μM. The obtained rates for the relatively slow phase were found to increase slightly with an increase in coenzyme concentration. In contrast to the experiments carried out with NADPH, no clear hyperbolic dependency was observed, although a trend is visible. This is in line with the fact that lowest measured concentration of (*R*)-NADPD (0.9 μM) was below the calculated $K_{d,NADPD}$ (0.7 μM). The maximum rate observed for the second phase was 2.0 $\pm$ 0.1 s^{-1}. This rate corresponds nicely with the reduction rate determined by monitoring the decrease in flavin absorbance (2.1 $\pm$ 0.1 s^{-1}; see above).

Binding of NADP$^+$ to Oxidized PAMO. The steady-state inhibition experiments with NADP$^+$ mentioned earlier indicated that the release of the oxidized coenzyme is the ultimate step in the catalytic cycle of PAMO as it acts as a competitive inhibitor. To gain insight into the process of NADP$^+$ release, we monitored the reverse reaction, i.e., the binding of the oxidized coenzyme to oxidized PAMO, by measuring spectral changes of the flavin upon titration of 66 μM PAMO with 0–514 μM NADP$^+$ (Figure 4A). Binding of NADP$^+$ results in a more resolved flavin spectrum which exhibits more prominent absorbance shoulders next to the maximum at 441 nm. Such a spectral effect hints about a more hydrophobic microenvironment around the flavin and is in line with the bound nicotinamide ring shielding the flavin from water. The largest decrease in absorbance was observed at 387 and 480 nm. At 387 nm, the decrease in absorption due to the formation of the E_{ox}–NADP$^+$ complex (ΔA_{387}) was 1830 M^{-1} cm^{-1}. This value was used to calculate the concentrations of the E_{ox}–NADP$^+$ complex and free NADP$^+$. By plotting the concentration of these two components against each other and fitting the data with eq 8 by means of linear regression, we determined the binding affinity toward the oxidized coenzyme [$K_{d,NADP^+}$ = 3.3 $\pm$ 0.3 μM (Figure 4B)]. This value is similar to the inhibition constant of NADP$^+$ ($K_{I,NADP^+}$ = 2.7 $\pm$ 1.0 μM).

$$K_d = \frac{[E_{ox} \cdot NADP^+]}{[E_{ox}]_{free} + [NADP^+]_{free}} \quad (8)$$

Kinetic analysis of the binding of NADP$^+$ by rapid mixing could not be carried out, as the absorption changes occurred within the dead time of the stopped-flow apparatus (<2 ms) using 5 μM PAMO and 25 μM NADP$^+$. This indicates that binding of NADP$^+$ to the oxidized enzyme is a fast process (>500 s^{-1}). In view of the binding constant, the rate of NADP$^+$ release also must be high ($k_{on}K_{d,NADP^+}$ > 66 s^{-1}), when compared with the steady-state turnover rate (k_{cat} = 3.1 s^{-1}).

Oxidative Half-Reaction. To monitor the reactions of reduced PAMO with molecular oxygen, 36 μM reduced PAMO was rapidly mixed with aerated buffer containing 36 μM NADP$^+$. This resulted in the formation of a spectral intermediate within 10 ms which displays an absorption maximum at ~380 nm (Figure 5A). Such spectral features are in line with formation of a C4a-peroxyflavin enzyme intermediate. As not enough data points could be acquired using the photodiode array detector for an accurate kinetic analysis, formation of the oxygenated enzyme intermediate was subsequently monitored using single-wavelength absorption measurements at 380 nm. The rate of C4a-peroxyflavin formation was measured using buffer containing 36 μM NADP$^+$ and several oxygen concentrations (250, 750, and 1250 μM). The observed rates, obtained by fitting the exponential absorption traces with eq 5, increased linearly with increasing concentrations of molecular oxygen. The pseudo-first-order rate constant describing the oxygenation of reduced PAMO (k_{ox}) was found to be 870 $\pm$ 35 mM^{-1} s^{-1} (Table 2). From this, it can be inferred that in aerated buffer (250 μM O_2) the C4a-peroxyflavin intermediate is formed at a rate of 220 s^{-1}, which is 70-fold higher than the k_{cat}. This indicates that during steady-state catalysis oxygenation of the reduced enzyme is not a rate-limiting step. In the absence of a suitable substrate, the formed C4a-peroxyflavin slowly decayed, yielding oxidized PAMO with

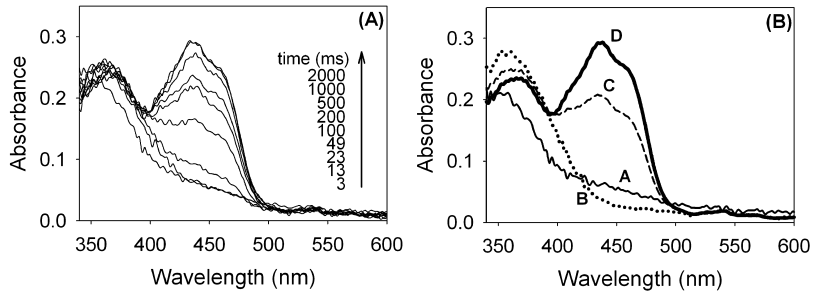

FIGURE 5: (A) Spectra of the reaction of NADPH-reduced wild-type PAMO and aerated buffer containing 1 mM phenylacetone (final concentration in the cell). The spectra shown were recorded at the indicated times. (B) Spectra of the deconvoluted enzyme species. By means of numerical integration (Pro-K, Applied Photophysics Ltd.), the spectra were derived using a three-step kinetic model (A → B → C → D), in which the first step corresponds to oxygenation of the reduced enzyme (110 s^{-1}, fixed), the second step represents the phenylacetone-dependent reoxidation of the enzyme (45 s^{-1}), and the third step presumably represents a conformational step (4.1 s^{-1}).

a rate of 0.01 s^{-1}. This rate is similar to the previously obtained uncoupling rate (k_{unc}) and suggests that the rate of NADPH consumption in the absence of a suitable substrate is mainly determined by the decay of the C4a-peroxyflavin intermediate.

The enzymatic Baeyer-Villiger oxidation has been suggested to occur by the nucleophilic attack of the C4a-peroxyflavin on organic substrates, yielding the so-called Criegee adduct. Thereafter, a rearrangement occurs, resulting in the formation of an ester/lactone product and the C4a-hydroxyflavin intermediate. Dehydration of the C4a-hydroxyflavin intermediate regenerates the oxidized flavin. To examine the spectral properties of the reaction intermediates and the rates at which they are formed, 36 μM anaerobic NADPH-reduced PAMO was mixed with aerated buffer containing phenylacetone (0.5–4 mM) as a substrate in the presence of 36 μM $NADP^+$ (Figure 5). Analysis of the obtained spectral scans revealed that the data could be fitted best with an irreversible three-step model (A → B → C → D). The spectral scans also showed that during the first step there is rapid formation of an enzyme species with isosbestic points at 340 and 420 nm and an absorption maximum at 380 nm. This step represents the oxygenation of the reduced flavin, and the corresponding rate is equal to the rate of the oxygenation of reduced PAMO in the absence of phenylacetone (870 mM^{-1} s^{-1}; see above). The formed peroxyflavin enzyme species is subsequently converted to the oxidized enzyme in two sequential steps. The observed rate of this kinetic event step increases hyperbolically with an increase in phenylacetone concentration. Fitting the experimental k_{obs} values with eq 6 reveals that this step occurs irreversibly at a rate (k_1) of 73 ± 1 s^{-1} and shows a half-saturation constant (K_{PA}) of 730 ± 50 μM. The last step is independent of the phenylacetone concentration and occurs at a constant rate of 4.1 ± 0.1 s^{-1} (k_2). This rate is similar to the catalytic rate of the enzyme (k_{cat} = 3.1 s^{-1}) and is most likely rate-limiting. The spectral properties of the final enzyme species resemble those of oxidized PAMO with bound $NADP^+$ (cf. Figure 4A), indicating that the final and relatively slow kinetic event (C → D) does not involve the release of the oxidized coenzyme as it still remains bound to the enzyme. This is in agreement with the kinetic data on $NADP^+$ binding reported above.

The oxidative half-reaction was also performed at various pH values (pH 6−9), in the presence of molecular oxygen and 1 mM phenylacetone. At all pH values that were measured, the obtained spectral data could be fitted best using

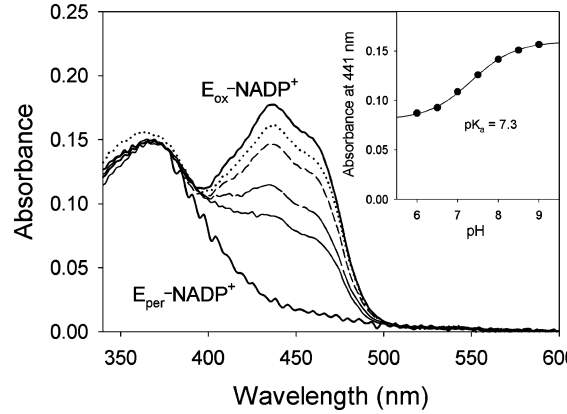

FIGURE 6: Spectra of the deconvoluted enzyme species observed during reoxidation of wild-type PAMO at various pH values. As previously shown in Figure 5B, the bold solid lines represent the spectra of the flavin C4a-peroxide intermediate and the reoxidized flavin with bound $NADP^+$, respectively. Some selected spectra of deconvoluted enzyme species C that were obtained at different pH values (pH 6.0, 7.0, 8.0, and 9.0) are shown as thin lines. The absorbance of this intermediate increased with an increase in pH, showing a pK_a of 7.3 (inset).

the same three-step model (A → B → C → D). The deconvoluted spectra of A (reduced flavin), B (peroxyflavin), and D (oxidized flavin) were shown not to be dependent on pH. This indicates that the pK_a of the peroxyflavin in PAMO falls outside the measured pH regime. Also, the rates of all transitions were hardly affected by pH. Only at pH 6–7 was the rate of decomposition of intermediate C found to decrease significantly (up to 4-fold). This is in line with the pH optimum for the activity of PAMO (>80% activity at pH 7–9) (*10*). Interestingly, the spectral characteristics of intermediate C were found to be highly dependent on pH (see Discussion). At low pH, the absorbance spectrum of the observed intermediate resembles that of a C4a-hydroxyflavin intermediate (*27, 28*), while at high pH, it resembles that of the fully oxidized enzyme with bound $NADP^+$ (Figure 6). In addition, the pH dependence of the absorption at 441 nm of this intermediate showed a pK_a of 7.3 (Figure 6, inset). These data suggest that at lower pH values the "C4a-hydroxy-FAD species" is relatively stable and accumulates during catalysis. A similar situation has been reported for eukaryotic flavin-containing monooxygenases (FMO), where a kinetic analysis has shown that dehydration of the C4a-hydroxyflavin intermediate is rate-limiting (*29*). Monitoring the A_{441} of PAMO during steady-state turnover at different pH values revealed a trend that was similar to the trend in

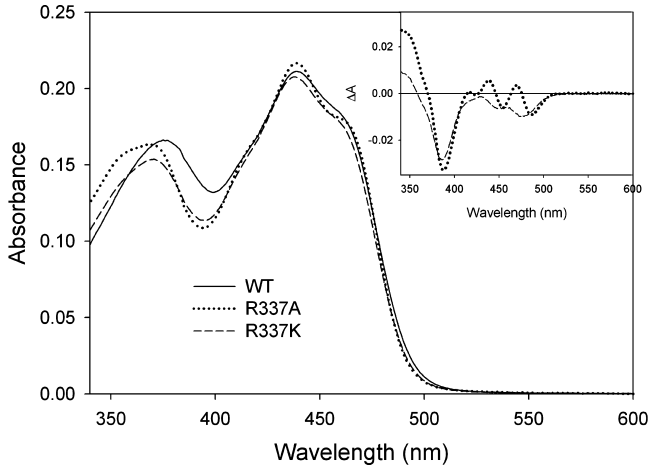

FIGURE 7: Flavin spectra of 17 μM wild-type PAMO (solid line), mutant R337A (dotted line), and mutant R337K (dashed line). The spectra were recorded in 50 mM Tris-HCl at pH 7.5 and 25 °C. The inset shows the difference spectra of both arginine mutants using wild-type PAMO as a reference.

the relative absorbance of intermediate C; the A_{441} during steady-state turnover was found to increase with an increase in pH. At pH 7.0, the absorption was found to be 43% of that of the fully oxidized enzyme, while at pH 8.5, this was 79%. These results are in line with the accumulation of intermediate C during catalysis, indicating that its decomposition is rate-limiting.

Mutants R337A and R337K. To elucidate the role of R337 in catalysis, we also investigated the kinetic properties of mutants R337A and R337K. The flavin absorption spectra of both mutants are somewhat different from that of wild-type PAMO with maxima at 370 and 441 nm for R337A and at 372 and 440 nm for R337K (Figure 7). In addition, mutant R337A shows a more pronounced shoulder at 460 nm. These results confirm that R337 is located near the isoalloxazine ring of the bound flavin cofactor, as suggested by the crystal structure of PAMO (*15*). Intriguingly, the spectral changes upon replacement of the arginine with an alanine closely resemble those changes induced upon binding of $NADP^+$ to wild-type PAMO, suggesting a more hydrophobic microenvironment around the flavin cofactor (Figure 7, inset).

Both R337 PAMO mutants showed a maximum NADPH consumption rate of 0.01 s^{-1} in aerated buffer in the presence of 10 mM phenylacetone. This rate is more than 300-fold lower than the catalytic rate of wild-type PAMO and also 5-fold lower than the uncoupling rate of wild-type PAMO. In the absence of phenylacetone, similar rates were obtained. Product analysis by means of gas chromatography revealed that no benzylacetate is formed using these PAMO mutants. When using benzylmethyl sulfide as a substrate, also no product formation was observed. This indicates that both mutants are unable to carry out Baeyer-Villiger oxidations or sulfoxidations. In contrast to that of wild-type PAMO, the A_{441} values of both mutants during steady state were very low (<1% of that of the fully oxidized enzyme), pointing to the accumulation of a reduced enzyme species.

Pre-steady-state kinetic studies of the reductive half-reaction of the R337A enzyme showed that this mutant has a relatively low reduction rate (Table 2). A similar low rate of flavin reduction was found for mutant R337K. NADPH fluorescence measurements showed that the R337A mutant has a similar affinity towards the nicotinamide coenzyme when compared with the wild-type enzyme with similar association and dissociation constants. These results show that replacement of the arginine at position 337 results in a drastic decrease of the reduction rate while the binding of NADPH is not affected.

The ability of both mutants to react with molecular oxygen after reduction by NADPH was also investigated. Mixing NADPH-reduced R337A PAMO with aerated buffer resulted in a rapid increase in absorption at 380 nm, which was observed for wild-type PAMO. By fitting the absorption traces with a single-exponential equation (eq 5), we obtained rates that increased linearly with an increase in O_2 concentration, resulting in a pseudo-first-order rate constant describing the oxygenation process. This indicates that R337 is not essential for the formation of the C4a-peroxyflavin intermediate. However, the oxygenation rate ($k_{ox,R337A}$) was found to be 20-fold lower than that of the wild type, suggesting that R337 plays an important role in the formation of the C4a-peroxyflavin intermediate. Again, similar results were found for mutant R337K. This shows that a lysine does not replace the functionality of the conserved R337. Decay of the peroxyflavin occurred at a rate of 0.001 s^{-1} for R337A and at a rate of 0.002 s^{-1} for R337K. These rates are in agreement with the observed rates of NADPH consumption under steady-state conditions.

DISCUSSION

Recent studies have shown that many bacterial and fungal genomes contain one or more BVMO genes (*21, 30*). This contrasts with the number of biochemically characterized BVMOs. BVMOs are often involved in degradation routes of aromatic or aliphatic ketones, while in some cases, they catalyze a crucial step in biosynthesis of a secondary metabolite. Biochemical studies on BVMOs have been limited by their limited availability, poor stability, and/or reluctance toward purification. For this reason, only CHMO has been studied in detail with respect to its catalytic and kinetic properties (*8, 9, 31, 32*). Unfortunately, it has proven to be impossible to obtain crystals of CHMO, prohibiting insight into the structural details of this BVMO. Recently, PAMO was identified by a genome database mining effort. The enzyme originates from a thermophilic bacterium, which explains the (thermo)stability of this enzyme, and it can be well expressed in *E. coli* (*10*). These features have triggered a number of biocatalytic studies that have shown that PAMO represents an interesting enzyme with respect to its potential use in synthetic chemistry (*12–14, 33*). Elucidation of the crystal structure of PAMO has provided valuable structural insight as it represents the only available BVMO structure (*15*). The identification of residues that form the active site cavity has enabled enzyme engineering studies that resulted in the design of several PAMO mutants that display significantly altered substrate specificities (*16, 19*). By performing steady-state and pre-steady-state kinetic studies, we have now elucidated the kinetic mechanism of PAMO. The next paragraphs highlight the observed features of the individual kinetic steps (Figure 8).

Reduction of the Flavin Cofactor. Our study shows that PAMO binds the reduced NADPH coenzyme with high

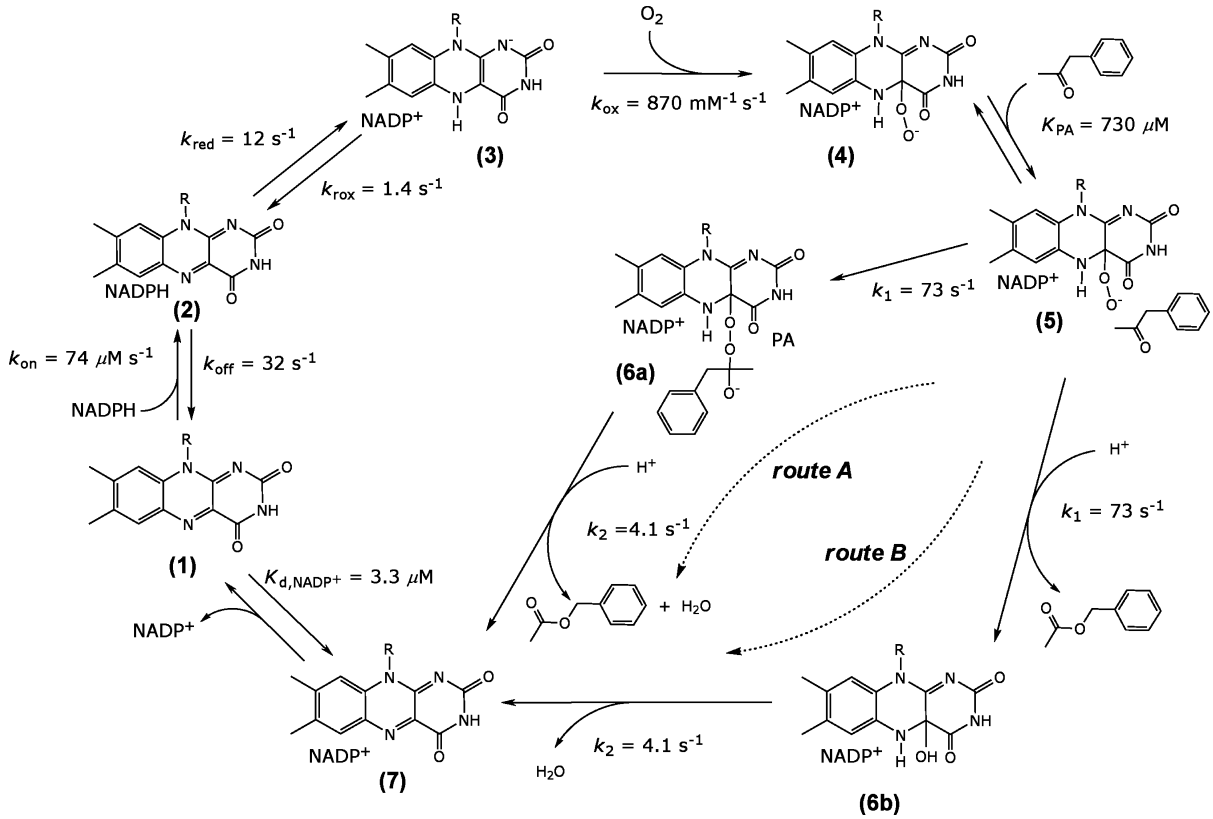

FIGURE 8: Proposed catalytic cycle for PAMO. The numbers in bold indicate the different observed flavin intermediates. The catalytic cycle starts with oxidized PAMO (**1**), which after binding NADPH (**2**) is reduced, yielding $NADP^+$ (**3**). The reduced enzyme is then oxygenated by molecular oxygen, resulting in the flavin C4a-peroxide intermediate (**4**). Binding of phenylacetone (**5**) leads to conversion into benzyl acetate. During the oxidation reaction, an enzyme intermediate is observed which may represent a Criegee intermediate (**6a**, route A) or a C4a-hydroxyflavin intermediate (**6b**, route B). A slow decay of the unassigned enzyme intermediate yields oxidized PAMO complexed with $NADP^+$. Release of $NADP^+$ completes the catalytic cycle. The individual rate constants and binding affinities appear beside the arrows.

affinity ($K_{d,NADPH}$ = 0.7 μM), after which reversible reduction of the bound flavin cofactor takes place (k_{red} = 11.8 s^{-1}; k_{rox} = 1.4 s^{-1}). By using deuterated NADPH, it was established that for reduction of PAMO, the nicotinamide (*R*)-hydrogen is transferred as a hydride from NADPH. Although such a specific hydride transfer was previously shown to occur in sequence-related FMOs (*34*), thus far no evidence was found that BVMOs reduce their cofactor by an enantioselective hydride transfer. This illustrates that binding and positioning of NADPH in PAMO are very specific, with the nicotinamide (*R*)-hydrogen in the proximity of the flavin cofactor. In contrast to several other flavin-containing monooxygenases, e.g., *p*-hydroxybenzoate hydroxylase (*35*), binding of phenylacetone is not required for effective reduction of the flavin cofactor by NADPH. This could indicate that binding of substrate occurs after reduction which is in line with the substrate concentration-dependent rate of oxygenation. Replacing the strictly conserved R337 with an alanine or lysine residue drastically reduces the rate of flavin reduction, while the affinity for NADPH is not altered. This indicates that R337 is involved in, for example, proper alignment of the reduced nicotinamide moiety with respect to the isoalloxazine part of the flavin cofactor and/or may modulate the redox properties of the flavin cofactor.

Oxygenation of the Reduced Flavin Cofactor (peroxyflavin formation). BVMOs owe their oxygenating activity to the fact that they can generate and stabilize the reactive C4a-peroxyflavin intermediate. As shown previously for CHMO and liver microsomal FMO (*9, 36*), we have also found that PAMO is able to form and stabilize such a flavin intermediate using the stopped-flow technique. The formation of the C4a-peroxyflavin intermediate (species **4** in Figure 8) upon oxygenation of reduced PAMO is a relatively fast process (k_{ox} = 870 mM^{-1} s^{-1}). However, it is worth noting that this rate is still considerably lower when compared with the rate of oxygenation of reduced CHMO, a closely related BVMO, which is oxygenated at a rate of ≥5000 mM^{-1} s^{-1} at 4 °C (*9*). With CHMO, it was observed that upon oxygenation initially a peroxyflavin form which exhibits an absorbance maximum at 366 nm is formed. Only in a relatively slow process (3.3 s^{-1}) was a species formed that absorbs most at 383 nm. It was concluded that the 366 nm species reflects the C4a-peroxyflavin species which can be protonated to form the C4a-hydroperoxyflavin intermediate. With PAMO, such a biphasic process is not seen: the peroxyflavin form is formed in a monophasic process and displays an absorption maximum at 380 nm. This suggests that in this case the C4a-hydroperoxyflavin intermediate is directly formed upon the reaction with molecular oxygen. This would imply that the pK_a of the peroxyflavin in PAMO is well above pH 7.5.

In the absence of substrate, the peroxy form of PAMO only slowly decays (0.01 s^{-1}) to form oxidized PAMO and hydrogen peroxide and thereby acts as an NADPH oxidase. The R337 mutants were also shown to be able to form the peroxyflavin, albeit with a decreased (~17-fold) oxygenation rate. Moreover, the mutants were able to stabilize this

oxygenated enzyme intermediate even better as only a relatively slow decay (0.001–0.002 s^{-1}) was observed. While it has been suggested that R337 would facilitate peroxyflavin formation and stabilization (*15*), this study shows that this active site residue is clearly not an absolute requirement for this. It appears that R337 is required to promote formation of a productive substrate−C4a-peroxyflavin complex. A similar role of an active site arginine in a flavoprotein monooxygenase has recently been reported (*37*). Elucidation of the crystal structure of 4-hydroxyphenylacetate 3-monooxygenase from *Thermus thermophilus* HB8 revealed that an arginine (R100) is involved in positioning the aromatic substrate, while it also is predicted to interact with the peroxy moiety of the C4a-hydroperoxyflavin. Whether R337 in PAMO is also involved in proper positioning of the reactants (including the bound $NADP^+$), formation of the Criegee adduct, and/or triggering of a conformational change, remains to be established. An interesting observation is the striking resemblance between the flavin spectrum of mutant R337A and that of wild-type PAMO with bound $NADP^+$. It suggests that upon binding of $NADP^+$, the conserved arginine moves away from the flavin, perhaps due to positive charge repulsion, creating an environment around the flavin that resembles that of mutant R337A. In line with this, alternate positions of the side chain of R337 have been observed in the crystal structure of PAMO (*15*).

Oxidation of Phenylacetone by the Peroxyflavin Intermediate. The reaction of the peroxyflavin intermediate with phenylacetone is a relatively fast and substrate-dependent process (K_{PA} = 730 μM; k_1 = 73 s^{-1}), while a kinetic event following this oxygenation reaction is relatively slow (k_2 = 4.1 s^{-1}) and limits the rate of catalysis. The spectral features of the enzyme intermediate that is formed upon oxygenation of phenylacetone are unusual. The exact nature of this intermediate could not be verified and awaits future study. However, the kinetic and spectral data suggest that the intermediate represents an oxygenated flavin intermediate. In fact, two possible scenarios for the observed intermediate are given in Figure 8: route A, in which a Criegee intermediate is formed, and route B, in which a hydroxyflavin intermediate is formed.

As formation of the unidentified enzyme intermediate is observed upon mixing reduced PAMO with substrate and oxygen, a likely candidate for this intermediate is a Criegee intermediate (route A, intermediate **6a** in Figure 8). Such an intermediate is predicted to be formed in any Baeyer-Villiger reaction but has never been observed experimentally. The kinetic data would suggest that the slow decay of this intermediate (k_2 = 4.1 s^{-1}), with concomitant product release, would determine the rate of catalysis. It was found that the spectral properties of the intermediate are strongly pH-dependent (pK_a of 7.3). Changing the pH, however, did not affect the rates of the observed events during the oxidative half-reaction, nor did it change the spectral features of the initially observed C4a-peroxyflavin enzyme intermediate. At pH 7.5, the unassigned intermediate spectrum resembles that of a mixture of an oxidized flavin and an oxygenated flavin species, while at high pH, the spectrum resembles that of fully oxidized flavin. These spectral features argue against a Criegee intermediate as it is unlikely that the Criegee intermediate would exhibit a flavin spectrum that is almost indistinguishable from that of oxidized flavin.

An alternative and, in our view, more likely interpretation of the data is indicated as route B in which the observed intermediate mainly represents a C4a-hydroxyflavin PAMO species at low pH (Figure 8). We propose that the pH-dependent spectral behavior reflects the protonation state of a residue in the active site of PAMO which is located close to the hydroxyl moiety of the C4a-hydroxyflavin form (**6b** in Figure 8). At low pH, the C4a-hydroxyflavin is stabilized to a great extent, yielding a spectrum which is similar to that of the C4a-hydroperoxyflavin. At high pH, the deprotonated active site residue destabilizes the C4a-hydroxyflavin intermediate, yielding oxidized PAMO in such a conformation that the formed water molecule is sequestered in the active site. Only a slow and pH-independent conformational change (k_2 = 4.1 s^{-1}) will result in formation of oxidized PAMO which is able to release the $NADP^+$ coenzyme. Such a conformational change would be in line with slight changes observed between the spectrum of the enzyme intermediate at high pH and the flavin spectrum of oxidized PAMO (Figure 6).

The rate constants derived from this kinetic study indicate that the decay of the unassigned enzyme intermediate (k_2) sets a limit for the k_{cat} value. $NADP^+$ binding measurements revealed that release of the oxidized coenzyme is a fast process ($k_{off,NADP^+}$ > 66 s^{-1}). Comparison of the determined steady-state kinetic parameters with the calculated steady-state kinetic parameters (see the Supporting Information) also shows a good correlation (Table 1). Previous studies with PAMO have shown that for a wide variety of organic substrates, similar k_{cat} values (2.0–3.6 s^{-1}) are measured (*13*). This suggests that the kinetic event associated with k_2 is not related to the chemical nature of the substrate or product. For the sequence-related liver microsomal FMO, it has been reported that the catalytic activity was determined by the slow decomposition of the C4a-hydroxyflavin intermediate, which is formed after the oxygenation of the organic substrate. In fact, also for this sequence-related monooxygenase, the decay of the peroxyflavin was found to occur in two phases (*27*). Also for CHMO, the oxidative half-reaction has been found to involve several phases. In this study, we show that reoxidation of PAMO occurs in two sequential steps, eventually yielding the oxidized enzyme complexed with $NADP^+$. The latter observation is in line with the high affinity of the enzyme for $NADP^+$ under the conditions in which the experiments were carried out.

Steady-state kinetic analysis of PAMO revealed that $NADP^+$ acts as a competitive inhibitor. This indicates that the oxidized nicotinamide coenzyme stays bound throughout the catalytic cycle. Such a tight enzyme−coenzyme interaction has also been observed for other sequence-related flavin-dependent monooxygenases (FMOs) and BVMOs (*8, 26, 29*). This suggests that the oxidized coenzyme may play a role in formation of one or more enzyme intermediates. In fact, it has been shown for PAMO that the bound coenzyme is required for enantioselective oxygenations. This suggests that the bound $NADP^+$ is involved in the proper positioning of the flavin cofactor and/or organic substrate (*38, 39*). By studying the binding of $NADP^+$ to CHMO, Sheng and coworkers (*9*) showed that a conformational change occurring prior to $NADP^+$ release is the rate-limiting step. However, for PAMO, we do not observe any kinetic behavior that would hint about a conformational change during coenzyme

binding or release. This again shows that the kinetic mechanism of PAMO clearly differs from CHMO while both enzymes show a significant level of sequence identity (40%).

In this study, we have shown that the catalytic rate of PAMO is limited by a kinetic event occurring in the penultimate step of the oxidative half-reaction. The observed spectral and kinetic data suggest that it reflects a conformational change in which the direct environment of the flavin cofactor is affected. Such a mechanism, which involves alternating conformations, resembles recurrent mechanistic features observed for other flavin-dependent monooxygenases (*40*). For aromatic hydroxylases and two-component monooxygenases, conformational dynamic events have been shown to be involved in the catalytic mechanism. It may reflect the way such enzymes have been able to combine several chemical reactions (flavin reduction, oxygenation of the flavin, oxygenation of an organic substrate, and dehydration of the flavin) in one or two active sites. A conformational change during the catalytic cycle of PAMO was also previously predicted on the basis of its crystal structure (*15*). In addition, we have identified the role of a crucial active site residue, which is essential for the catalytic activity of PAMO, R337. This arginine, which is conserved in all other type I BVMOs, is required not only for proper reduction and oxygenation of the flavin cofactor but also for the reaction of the C4a-peroxyflavin intermediate with organic substrates.

SUPPORTING INFORMATION AVAILABLE

Data for the reductive half-reaction using NADPD and computation of the steady-state kinetic parameters using the determinant method (*41*). This material is available free of charge via the Internet at http://pubs.acs.org.

REFERENCES

1. Kamerbeek, N. M., Janssen, D. B., van Berkel, W. J. H., and Fraaije, M. W. (2003) Baeyer-Villiger monooxygenases, an emerging family of flavin-dependent biocatalysts. *Adv. Synth. Catal. 345*, 667–678.
2. Reetz, M. T., Brunner, B., Schneider, T., Schulz, F., Clouthier, C. M., and Kayser, M. M. (2004) Directed evolution as a method to create enantioselective cyclohexanone monooxygenases for catalysis in Baeyer-Villiger reactions. *Angew. Chem., Int. Ed. 43*, 4075–4078.
3. Cheesman, M. J., Kneller, M. B., Kelly, E. J., Thompson, S. J., Yeung, C. K., Eaton, D. L., and Rettie, A. E. (2001) Purification and characterization of hexahistidine-tagged cyclohexanone monooxygenase expressed in *Saccharomyces cerevisiae* and *Escherichia coli*. *Protein Expression Purif. 21*, 81–86.
4. Donoghue, N. A., Norris, D. B., and Trudgill, P. W. (1976) The purification and properties of cyclohexanone oxygenase from *Nocardia globerula* CL1 and *Acinetobacter* NCIB 9871. *Eur. J. Biochem. 63*, 175–192.
5. Baldwin, C. V., and Woodley, J. M. (2006) On oxygen limitation in a whole cell biocatalytic Baeyer-Villiger oxidation process. *Biotechnol. Bioeng. 95*, 362–369.
6. Mihovilovic, M. D., Rudroff, F., Winninger, A., Schneider, T., Schulz, F., and Reetz, M. T. (2006) Microbial Baeyer-Villiger oxidation: Stereopreference and substrate acceptance of cyclohexanone monooxygenase mutants prepared by directed evolution. *Org. Lett. 8*, 1221–1224.
7. Cheesman, M. J., Kneller, M. B., and Rettie, A. E. (2003) Critical role of histidine residues in cyclohexanone monooxygenase expression, cofactor binding and catalysis. *Chem.-Biol. Interact. 146*, 157–164.
8. Ryerson, C. C., Ballou, D. P., and Walsh, C. (1982) Mechanistic studies on cyclohexanone oxygenase. *Biochemistry 21*, 2644–2655.
9. Sheng, D., Ballou, D. P., and Massey, V. (2001) Mechanistic studies of cyclohexanone monooxygenase: Chemical properties of intermediates involved in catalysis. *Biochemistry 40*, 11156–11167.
10. Fraaije, M. W., Wu, J., Heuts, D. P. H. M., van Hellemond, E. W., Lutje Spelberg, J. H., and Janssen, D. B. (2004) Discovery of a thermostable Baeyer-Villiger monooxygenase by genome mining. *Appl. Microbiol. Biotechnol. 66*, 393–400.
11. Fraaije, M. W., Kamerbeek, N. M., Heidekamp, A. J., Fortin, R., and Janssen, D. B. (2004) The prodrug activator EtaA from *Mycobacterium tuberculosis* is a Baeyer-Villiger monooxygenase. *J. Biol. Chem. 279*, 3354–3360.
12. de Gonzalo, G., Torres Pazmiño, D. E., Ottolina, G., Fraaije, M. W., and Carrea, G. (2005) Oxidations catalyzed by phenylacetone monooxygenase from *Thermobifida fusca*. *Tetrahedron Asymmetry 16*, 3077–3083.
13. Schulz, F., Leca, F., Hollmann, F., and Reetz, M. T. (2005) Towards practical biocatalytic Baeyer-Villiger reactions: Applying a thermostable enzyme in the gram-scale synthesis of optically-active lactones in a two-liquid-phase system. *Beilstein J. Org. Chem.,* 1.
14. de Gonzalo, G., Ottolina, G., Zambianchi, F., Fraaije, M. W., and Carrea, G. (2006) Biocatalytic properties of Baeyer-Villiger monooxygenases in aqueous-organic media. *J. Mol. Catal. B: Enzym. 39*, 91–97.
15. Malito, E., Alfieri, A., Fraaije, M. W., and Mattevi, A. (2004) Crystal structure of a Baeyer-Villiger monooxygenase. *Proc. Natl. Acad. Sci. U.S.A. 101*, 13157–13162.
16. Bocola, M., Schulz, F., Leca, F., Vogel, A., Fraaije, M. W., and Reetz, M. T. (2005) Converting phenylacetone monooxygenase into phenylcyclohexanone monooxygenase by rational design: Towards practical Baeyer-Villiger monooxygenases. *Adv. Synth. Catal. 347*, 979–986.
17. Clouthier, C. M., Kayser, M. M., and Reetz, M. T. (2006) Designing new Baeyer-Villiger monooxygenases using restricted CASTing. *J. Org. Chem. 71*, 8431–8437.
18. Kayser, M. M., and Clouthier, C. M. (2006) New bioorganic reagents: Evolved cyclohexanone monooxygenase—Why is it more selective? *J. Org. Chem. 71*, 8424–8430.
19. Torres Pazmiño, D. E., Snajdrova, R., Rial, D. V., Mihovilovic, M. D., and Fraaije, M. W. (2007) Altering the substrate specificity and enantioselectivity of phenylacetone monooxygenase by structure-inspired enzyme redesign. *Adv. Synth. Catal. 349*, 1361–1368.
20. Kamerbeek, N. M., Moonen, M. J. H., van Der Ven, J. G. M., van Berkel, W. J. H., Fraaije, M. W., and Janssen, D. B. (2001) 4-Hydroxyacetophenone monooxygenase from *Pseudomonas fluorescens* ACB. *Eur. J. Biochem. 268*, 2547–2557.
21. Torres Pazmiño, D. E., and Fraaije, M. W. (2007) Discovery, redesign and applications of Baeyer-Villiger monooxygenases, in *Future Directions in Biocatalysis* (Matsuda, T., Ed.) pp 107–128, Elsevier, Amsterdam.
22. Kamerbeek, N. M., Fraaije, M. W., and Janssen, D. B. (2004) Identifying determinants of NADPH specificity in Baeyer-Villiger monooxygenases. *Eur. J. Biochem. 271*, 2107–2116.
23. Jeong, S.-S., and Gready, J. E. (1994) A method of preparation and purification of (4*R*)-deuterated-reduced nicotinamid adenine dinucleotide phosphate. *Anal. Biochem. 221*, 273–277.
24. Kamerbeek, N. M., Olsthoorn, A. J. J., Fraaije, M. W., and Janssen, D. B. (2003) Substrate specificity and enantioselectivity of 4-hydroxyacetophenone monooxygenase. *Appl. Environ. Microbiol. 69*, 419–426.
25. Fersht, A. (1999) *Structure and Mechanism in Protein Science: A Guide to Enzyme Catalysis and Protein Folding*, Freeman, New York.
26. van den Heuvel, R. H. H., Tahallah, N., Kamerbeek, N. M., Fraaije, M. W., van Berkel, W. J. H., Janssen, D. B., and Heck, A. J. R. (2005) Coenzyme binding during catalysis is beneficial for the stability of 4-hydroxyacetophenone monooxygenase. *J. Biol. Chem. 280*, 32115–32121.
27. Jones, K. C., and Ballou, D. P. (1986) Reactions of the 4a-hydroperoxide of liver microsomal flavin-containing monooxygenase with nucleophilic and electrophilic substrates. *J. Biol. Chem. 261*, 2553–2559.
28. Entsch, B., Ballou, D. P., and Massey, V. (1976) Flavin-oxygen derivatives involved in hydroxylation by p-hydroxybenzoate hydroxylase. *J. Biol. Chem. 251*, 2550–2563.
29. Poulsen, L. L., and Ziegler, D. M. (1995) Multisubstrate flavin-containing monooxygenases: Applications of mechanism to specificity. *Chem.-Biol. Interact. 96*, 57–73.

30. McLeod, M. P., Warren, R. L., Hsiao, W. W. L., Araki, N., Myhre, N., Fernandes, C., Miyazawa, D., Wong, W., Lillquist, A. L., Wang, D., Dosanjh, M., Hara, H., Petrescu, A., Morin, R. D., Yang, G., Stott, J. M., Schein, J. E., Shin, H., Smailus, D., Siddiqui, A. S., Marra, M. A., Jones, S. J. M., Holt, R., Brinkman, F. S. L., Miyauchi, K., Fukuda, M., Davies, J. E., Mohn, W. W., and Eltis, L. D. (2006) The complete genome of *Rhodococcus* sp. RHA1 provides insights into a catabolic powerhouse. *Proc. Natl. Acad. Sci. U.S.A. 103*, 15582–15587.
31. Bennett, A. (2004) Mechanism of oxidative inactivation of *Acinetobacter* sp. NCIMB 9871 cyclohexanone monooxygenase. *J. Undergrad. Chem. Res. 6.*
32. Ottolina, G., de Gonzalo, G., and Carrea, G. (2005) Theoretical studies of oxygen atom transfer from flavin to electron-rich substrates. *THEOCHEM 757*, 175–181.
33. Riva, S., Fassi, P., Allegrini, P., and Razzetti, G. (2008) Process for the preparation of (−)-modafinil. U.S. Patent 7316918.
34. Beaty, N. B., and Ballou, D. P. (1981) The reductive half-reaction of liver microsomal FAD-containing monooxygenase. *J. Biol. Chem. 256*, 4611–4618.
35. Entsch, B., and van Berkel, W. J. H. (1995) Structure and mechanism of para-hydroxybenzoate hydroxylase. *FASEB J. 9*, 476–483.
36. Beaty, N. B., and Ballou, D. P. (1981) The oxidative half-reaction of liver microsomal FAD-containing monooxygenase. *J. Biol. Chem. 256*, 4619–4625.
37. Kim, S. H., Hisano, T., Takeda, K., Iwasaki, W., Ebihara, A., and Miki, K. (2007) Crystal structure of the oxygenase component (HpaB) of the 4-hydroxyphenylacetate 3-monooxygenase from *Thermus thermophilus* HB8. *J. Biol. Chem. 282*, 33107–33117.
38. Hollmann, F., Taglieber, A., Schulz, F., and Reetz, M. T. (2007) A light-driven stereoselective biocatalytic oxidation. *Angew. Chem., Int. Ed. 46*, 2903–2906.
39. de Gonzalo, G., Ottolina, G., Carrea, G., and Fraaije, M. W. (2005) $[Cp^*Rh\ (bpy)(H_2O)]^{2+}$ as coenzyme substitute in enzymatic oxidations catalyzed by Baeyer-Villiger monooxygenases. *Chem. Commun. 29*, 3724–3726.
40. van Berkel, W. J. H., Kamerbeek, N. M., and Fraaije, M. W. (2006) Flavoprotein monooxygenases, a diverse class of oxidative biocatalysts. *J. Biotechnol. 124*, 670–689.
41. Huang, C. Y. (1983) Derivation of initial velocity and isotope exchange rate equations, in *Contemporary Enzyme Kinetics and Mechanism* (Purich, D., Ed.) 2nd ed., pp 54–84, Academic Press, Inc., New York.

BI702296K